16th World Congress in Computational Mechanics (WCCM)
21-26 July 2024, Vancouver, Canada
A. Korobenko, M. Laforest, S. Prudhomme, R. Vaziri (Eds)

DUAL-WEIGHTED RESIDUAL GOAL-ORIENTED ERROR ESTIMATION FOR TEMPORAL ADAPTIVITY IN PHASE-FIELD FRACTURE

V. KOSIN[1], A. FAU[1], F. HILD[1] AND T. WICK[2,1]

[1] Université Paris-Saclay, CentraleSupélec, ENS Paris-Saclay, CNRS
LMPS – Laboratoire de Mécanique Paris-Saclay
Gif-sur-Yvette, France
{viktor.kosin,amelie.fau,francois.hild}@ens-paris-saclay.fr

[2] Leibniz University Hannover, Institute of Applied Mathematics
Hannover, Germany
thomas.wick@ifam.uni-hannover.de

Key words: Phase-field fracture, Goal-oriented temporal adaptivity, Space–time finite elements, Dual-weighted residual method, Single edge notched tensile test

Abstract. This work focuses on temporal adaptivity for phase-field fracture problems. The methodology requires a space-time formulation and utilizes a space-time Galerkin finite element discretization for the governing phase-field equations. Then, goal functionals (i.e., quantities of interest) are introduced. The computational implementation of goal-oriented error control employs the dual-weighted residual method in which an adjoint problem must be solved. As the analysis is quasi-static, without a temporal derivative, the adjoint problem of the quasi-static primal problem decouples in time. Nonetheless, time-averaged goal functionals can also be considered. The temporal errors are localized using a partition of unity, which allows one to adaptively refine and coarsen the time intervals in the space-time cylinder. Numerical tests are performed on a single edge notched tensile test to investigate the quality of the proposed error estimator.

1 Introduction

Modeling fracture problems with a phase-field approach is currently of great interest [1, 6–8, 13, 17, 29]. One characteristic feature (besides several others) in many numerical and practical examples is that fractures often first initiate or slowly develop from a given location, and then grow fast or brutally. This behavior naturally calls for different time step sizes in order to keep the computational cost reasonable while ensuring a certain accuracy of the numerical solution. Besides ad-hoc choices and a priori information for choosing the time step sizes, heuristic error estimators or mathematically derived a posteriori error estimators may be employed. Clearly, the last mentioned class of error estimators usually performs best as it is derived by taking the

mathematical structure of the governing equations into account. Yet, these developments are often costly in terms of derivation, implementation, and verification.

As previosuly mentioned, the topic of this work is on temporal error estimation. In terms of phase-field fracture, the following studies have been made so far. The quality of the step size was based on a stability analysis for explicit time discretization in rate-dependent phase-field fracture [30]. Step sizes were controlled based on the number of Newton iterations needed in the previous step [18] or the slope of the energy curve of sub-steps [14]. Very recently, the so-called Efendiev & Mielke scheme was applied to phase-field fracture [21], and finally a goal-oriented heuristic error estimator was developed [28, Section 9.6].

The objective of the present study is to develop an a posteriori goal-oriented temporal error estimator, which is employed after error localization for adaptive temporal refinement and coarsening. One successful possibility is to use the dual-weighted residual method [4]. Therein, an adjoint problem must be solved, which is linear, but running backward in time. A specific characteristics of phase-field fracture is that two PDEs couple, namely, displacements and phase-field variable, where the latter is subject to an inequality constraint in time. The overall problem is a coupled variational inequality system [28]. Thus, developing goal-oriented error control with the dual-weighted residual method requires some care and ideas can be taken from early works [19, 24] as well as recent ones for spatial goal-oriented adaptivity with phase-field [26, 27]. More specifically, one starts from a space-time formulation in a space-time cylinder. This formulation allows Galerkin finite elements to be employed in space and time, where the latter is of interest; the reason being that one can use a posteriori estimates known for finite elements and apply them to the temporal direction. Such space-time estimates with the dual-weighted residual method are known for full space-time adaptivity [5, 22, 23, 25] (not yet phase-field though), and more specifically for temporal adaptivity, let us mention Refs. [9, 15, 16].

The outline of the paper is as follows. In Section 2, the space-time formulation of phase-field fracture is introduced. Section 3 addresses the finite element discretization of the weak form and Section 4 gives an overview of the dual-weighted residual method, which is used to construct the goal-oriented error estimator. The partition-of-unity localization of the error estimator is given in Section 5. The performance of the error estimator and the temporal adaptivity are studied in Section 6.

2 Space-Time Formulation of Phase-Field Fracture

For the space-time formulation of phase-field fracture in a weak form, some basic notations and required spaces are introduced. Throughout this paper, $\Omega \subset \mathbb{R}^d$ is considered to be a bounded domain and $\mathcal{I} = (0, T)$ is considered to be a compact time interval, such that $\Omega \times \mathcal{I}$ forms the space-time cylinder. Further,

$$H^1_D(\Omega;\mathbb{R}^d) := \left\{ \boldsymbol{u} \in H^1(\Omega,\mathbb{R}^d) : \boldsymbol{u}|_{\Gamma_D} = 0 \text{ with } \Gamma_D \subset \partial\Omega \right\},$$
$$\mathcal{V} := H^1_D(\Omega;\mathbb{R}^d) \times H^1(\Omega),$$

and

$$\mathcal{X} := \Big\{ U = (\boldsymbol{u}, \varphi) : U \in L^2(\mathcal{I}, \mathcal{V}), \partial_t \varphi \in L^2(\mathcal{I}, H^1(\Omega)^*) \text{ and } \varphi \text{ satisfies} \\ \text{the weak irreversibility condition } (\partial_t \varphi, \psi)_{\Omega \times \mathcal{I}} \leq 0 \text{ for all } \psi \in L^2(\mathcal{I}; H^1(\Omega)) \Big\},$$

where

$$(U, V)_{\Omega \times \mathcal{I}} := \int_{\mathcal{I}} \int_{\Omega} U \cdot V \, \mathrm{d}x \, \mathrm{d}t.$$

Last, the weak form can be formulated as follows. For given initial values $U_0 = (u_0, \varphi_0) \in \mathcal{V}$, find $U = (\boldsymbol{u}, \varphi) \in \mathcal{X}$ such that it holds for $\Xi := \{0, \varphi\}$

$$A(U)(\Phi - \Xi) \geq 0 \quad \forall \Phi := (\boldsymbol{\phi}^{\boldsymbol{u}}, \phi^{\varphi}) \in \mathcal{X}, \tag{1}$$

where

$$A(U)(\Phi) := \left(g(T(\varphi))\boldsymbol{\sigma}^+(\boldsymbol{u}) + \boldsymbol{\sigma}^-(\boldsymbol{u}), \boldsymbol{\varepsilon}(\boldsymbol{\phi}^u)\right)_{\Omega \times \mathcal{I}} + (1 - \kappa) \left(\varphi \boldsymbol{\sigma}^+(\boldsymbol{u}) : \boldsymbol{\varepsilon}(\boldsymbol{u}), \phi^{\varphi}\right)_{\Omega \times \mathcal{I}} \\ + \frac{G_c}{\ell} \left(1 - \varphi, \phi^{\varphi}\right)_{\Omega \times \mathcal{I}} + G_c \ell \left(\nabla \varphi, \nabla \phi^{\varphi}\right)_{\Omega \times \mathcal{I}}$$

and $T(\varphi)$ is an approximation of φ.

3 Discretization

The space-time cylinder $\Omega \times \mathcal{I}$ is discretized using tensor-product space-time finite elements. Piecewise constant functions are chosen in time. Due to the discontinuous discretization in time, the primal problem is solved using a time-stepping scheme. In space, an H^1 conforming discrete space $\mathcal{X}_h \subset \mathcal{X}$ consisting of biquadratic functions on quadrilateral elements is introduced. Therefore, the extrapolation as well as the active set method [11] are chosen for the approximation $T(\varphi)$, and as a solution algorithm for the inequality in Equation (1), respectively. Let $\mathcal{A} = \mathcal{A}(t)$ be the active set at time $t \in \mathcal{I}$ and $\Xi_h = (0, \xi_h^{\varphi}) \in \mathcal{X}_h$, one can replace $\mathcal{X}_h$ in Equation (1) by

$$\mathcal{K}^{\mathcal{A}}_{\Xi_h}(t) := \{ U_h = (\boldsymbol{u}_h, \varphi_h) \in \mathcal{V}_h : \varphi_h(\boldsymbol{x}, t) = \xi_h^{\varphi}(\boldsymbol{x}, t) \text{ for almost all } \boldsymbol{x} \in \mathcal{A}(t) \}$$

and the time discrete problem to be solved at each time t_k reads as follows. For given $\Xi_{hk-1} := \{0, \varphi_{hk-1}\} \in \mathcal{V}_h$ and active set $\mathcal{A}$, find $U_{hk} = (\boldsymbol{u}_{hk}, \varphi_{hk}) \in \mathcal{K}^{\mathcal{A}}_{\Xi_{hk-1}}(t_k)$ such that it holds

$$A(U_{hk})(\Phi_{hk}) = 0 \quad \forall \Phi_{hk} := (\boldsymbol{\phi}^{\boldsymbol{u}}_{hk}, \phi^{\varphi}_{hk}) \in \mathcal{K}^{\mathcal{A}}_0(t_k). \tag{2}$$

4 Dual-Weighted Residual Error Estimation

In this section, given a target functional $J : \mathcal{X} \to \mathbb{R}$, the evaluation of the temporal error $J(U_h) - J(U_{hk})$ is investigated, where U_h is the semi-discrete spatial solution. One notes that U_h

is assumed to be sufficiently accurate in order to neglect spatial discretization errors. Following Ref. [4], a constrained optimization problem is formulated

$$\min J(U_h) - J(U_{hk}) \quad \text{s.t.} \quad A(U_h)(\Phi_h - \Xi_h) \geq 0 \quad \forall \Phi_h \in \mathcal{X}.$$

Assuming that for some $\Xi_h = (0, \xi_h^{\varphi}) \in \mathcal{X}_h$ one can again determine an active set $\mathcal{A}$ such that $U_h(t) \in \mathcal{K}_{\Xi,h}^{\mathcal{A}}(t)$ for almost all $t \in \mathcal{I}$, the inequality is replaced and the new problem reads

$$\min J(U_h) - J(U_{hk}) \quad \text{s.t.} \quad A(U_h)(\Phi_h) = 0 \quad \forall \Phi_h \in \mathcal{K}_{\Xi,h}^{\mathcal{A}}(t). \tag{3}$$

With the help of the Lagrangian $L : \mathcal{K}_{\Xi,h}^{\mathcal{A}} \times \mathcal{K}_{0,h}^{\mathcal{A}} \to \mathbb{R}$ defined as

$$L(U_h, Z_h) := (J(U_h) - J(U_{hk})) - A(U_h)(Z_h),$$

and the Lagrange multiplier $Z_h \in \mathcal{K}_{0,h}^{\mathcal{A}}$, the constrained optimization problem (3) is transformed into the following saddle point problem

$$L'_U(U_h, Z_h) = J'(U_h)(\Phi_h) - A'_U(U_h)(\Phi_h, Z_h) = 0, \tag{4}$$
$$L'_Z(U_h, Z_h) = -A(U_h)(\Phi_h) = 0. \tag{5}$$

Additionally to the primal problem, one also has to solve a dual problem (Equation (4)). Based on Ref. [4], the error representation reads

$$J(U_h) - J(U_{hk}) = \frac{1}{2}\rho(U_h)(Z_h - Z_{hk}) + \frac{1}{2}\rho^*(U_h)(U_h - U_{hk}, Z_{hk}) + \mathcal{R}^{(3)},$$

where

$$\rho(U_h)(Z_h - Z_{hk}) := -A(U_h)(Z_h - Z_{hk}),$$
$$\rho^*(U_h)(U_h - U_{hk}, Z_{hk}) := J'(U_h)(U_h - U_{hk}) - A'_U(U_h)(U_h - U_{hk}, Z_{hk}),$$

and $\mathcal{R}^{(3)}$ is a remainder term of order 3. Unfortunately, U_h and Z_h are not computationally accessible as they are only discrete in space and still continuous in time. In this work, they are approximated by solving the primal problem and the dual problem on temporal discretizations that have twice as many time steps as the original discretization. The temporal estimator is finally defined as

$$\eta := \frac{1}{2}\rho(U_h)(Z_h - Z_{hk}) + \frac{1}{2}\rho^*(U_h)(U_h - U_{hk}, Z_{hk}). \tag{6}$$

5 Partition-of-Unity Localization and Adaptivity

The estimator defined in Equation (6) is still in a global form. In the following, it is localized by a partition of unity [20, 25]. Let $\mathcal{V}_{\text{PU}} = \{\chi_k\}_k$ be a one dimensional, continuous finite element discretization with piecewise linear functions, then it holds $\sum \chi_k \equiv 1$, and a local estimator is defined as

$$\eta_k := \frac{1}{2}\rho(U_h)((Z_h - Z_{hk})\chi_k) + \frac{1}{2}\rho^*(U_h)((U_h - U_{hk})\chi_k, Z_{hk}).$$

The error for a time element τ is then computed by adding the values of all η_k that have a positive support on τ. For the next section, the error at time t_k reads

$$\eta_{\delta_k} := \frac{1}{2}\rho(U_h)((Z_h - Z_{hk})\delta_k) + \frac{1}{2}\rho^*(U_h)((U_h - U_{hk})\delta_k, Z_{hk}), \tag{7}$$

where δ is the Dirac delta function, and $\delta_k = \delta(t_k)$.

6 Numerical Experiments

The dual-weighted residual method described in the previous sections was implemented by extending the open-source software `pfm-cracks` [10], which is based on the finite-element library `deal.ii` [2, 3]. Furthermore, the implementation of the space-time formulation was inspired by Refs. [12, 25].

6.1 Investigated configuration

A single edge notched tensile test is used to illustrate the method. In this test, the top boundary Γ_1 of the sample (Figure 1) is pulled at a velocity of $1\ \mathrm{mm\,s^{-1}}$ for 65×10^{-4} s.

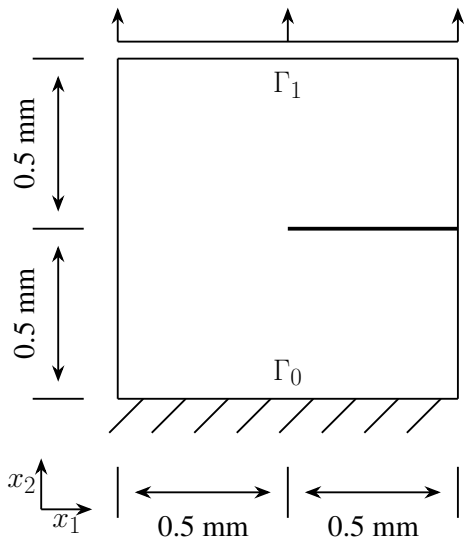

Figure 1: Geometry of the sample and applied boundary conditions.

6.2 Goal functionals

The goal functional is chosen to be the mean normal tractions at the boundary Γ_1. Therefore, $J(U)$ and its evaluation at some specific time points t_k denoted by $J_k(U)$ are defined as

$$J(U) := \int_{\mathcal{I}}\int_{\Gamma_1} -\boldsymbol{\sigma}(\boldsymbol{u})\boldsymbol{n}\cdot\boldsymbol{n}\,\mathrm{d}s\,\mathrm{d}t \quad \text{and} \quad J_k(U) := \int_{\Gamma_1} -\boldsymbol{\sigma}(\boldsymbol{u}(t_k))\boldsymbol{n}\cdot\boldsymbol{n}\,\mathrm{d}s\,\mathrm{d}t. \tag{8}$$

One is interested in the goal functional values themselves as well as their temporal errors defined by

$$J(U_h) - J(U_{hk}), \qquad J_k(U_h) - J_k(U_{hk}).$$

It is noteworthy that the spatial discretization is chosen sufficiently fine such that spatial discretization errors are assumed negligible.

6.3 Discussion

By comparing the phase-field solution for the initial temporal discretization and the discretization after 4 global refinements in time (Figure 2), a significant increase is observed for the speed of crack propagation, indicating that the approximation $T(\varphi)$ and the time step size has a significant impact on the quality of the solution itself. While the crack just started to initiate at the end of the simulation for the initial discretization, the crack already propagated through a significant part of the sample width for the final discretization.

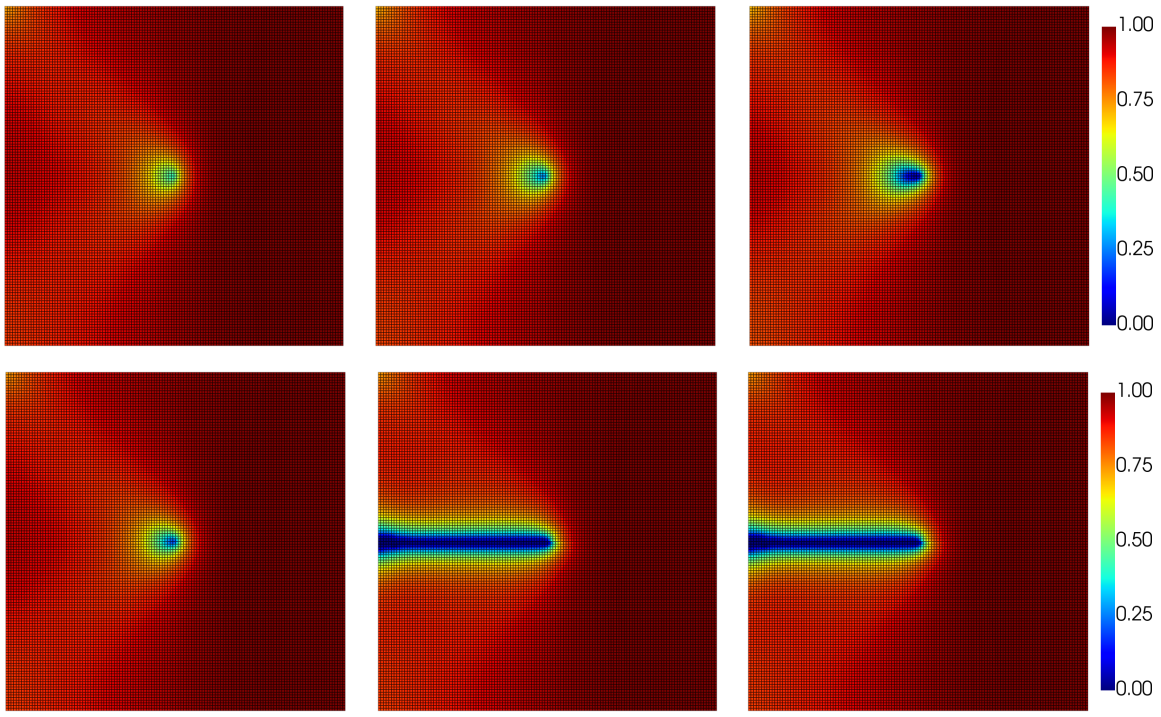

Figure 2: Phase-field solutions at times $t = 58 \cdot 10^{-4}$ s, $60 \cdot 10^{-4}$ s, $62 \cdot 10^{-4}$ s (left to right) for the initial time discretization (top) and after 4 global refinements (bottom).

More insight is gained by comparing the instantaneous goal functional values shown in Figure 3. In the linear elastic phase, the values match for all refinement levels, and the levels only differ once the crack starts to propagate. Therefore, in the beginning, a coarse temporal discretization is sufficient while fine time steps should be chosen during crack propagation.

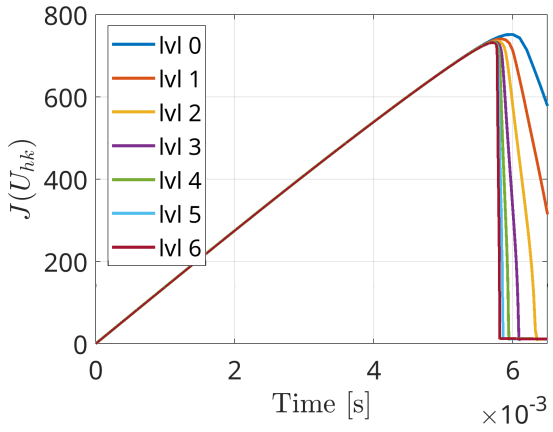

Figure 3: Mean normal traction with different temporal discretization levels.

To investigate the quality of the error estimator, the solution after 6 global refinements is chosen to be the reference. This choice allows the 'true' error $J(U_h) - J(U_{hk})$ to be computed as well as the effectivity index I_{eff} defined as

$$I_{\text{eff}} := \left| \frac{\eta}{J(U_h) - J(U_{hk})} \right| .$$

For every refinement level, the goal value, the exact error, the estimated error and the error indicators are summarized in Table 1. While the error estimator underestimates the actual error throughout the different levels, it clearly improves for finer levels and it seems that asymptotically $I_{\text{eff}} \to 1$. Considering the nonlinearities and temporal discontinuities of the phase-field fracture model, this result is very promising.

Table 1: Estimated error, exact error and error indicators for different levels of adaptive refinement and coarsening of the temporal meshes. The goal value of the reference discretization is 2.261.

Ref. Level	0	1	2	3	4
$J(U_{hk})$	2.782	2.675	2.511	2.393	2.324
$J(U_h) - J(U_{hk})$	0.492	0.406	0.250	0.132	0.063
η	0.0465	0.0811	0.064	0.040	0.027
I_{eff}	0.085	0.187	0.222	0.249	0.305

By comparing the temporal point error $J_k(U_h) - J_k(U_k)$, where $J_k(\cdot)$ denotes the evaluation of $J(\cdot)$ at the temporal point t_k, (Equation (8)), with the temporal point value of the error estimator η_{δ_k} (Equation (7)), it is observed that with each refinement, the localization becomes better as well. Interestingly, the error just after crack initiation is underestimated the most, see Figure 4. Instead of estimating an immediate jump in the error, the error is always estimated to gradually increase.

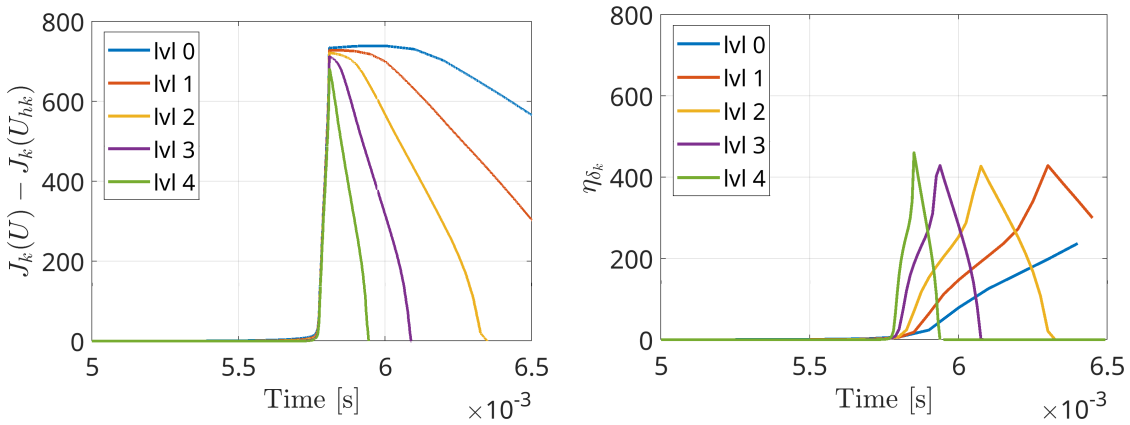

Figure 4: Zoomed in view of the exact error (left) and the estimated error (right) for globally refined temporal meshes.

In Figure 5, the step sizes are shown for different levels of adaptive refinement and coarsening, which are controlled by the estimator. A time step is refined if the local error is greater than 50% of the average error per time step and two neighboring time steps are combined if the local error on both elements is less than 5% of the average error per time step.

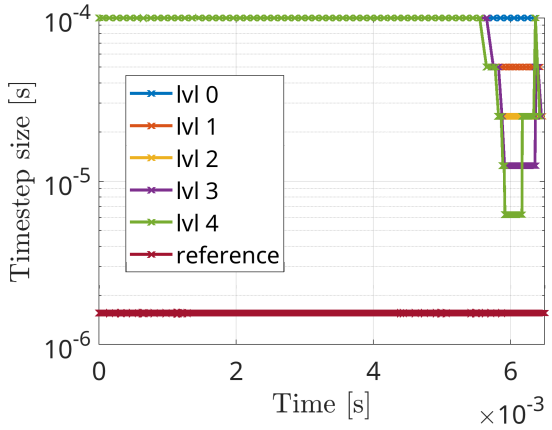

Figure 5: Time step sizes after different adaptive refinements cycles.

Using this strategy, the time steps are refined when the mean normal traction drops (i.e., the crack propagates), and they are coarsened once the crack has propagated and the normal traction is essentially equal to zero. Since the estimated error is very low compared to the exact error at crack initiation, the refinement in this period of time only starts after number of refinement levels, more precisely at level 4 (Figure 6).

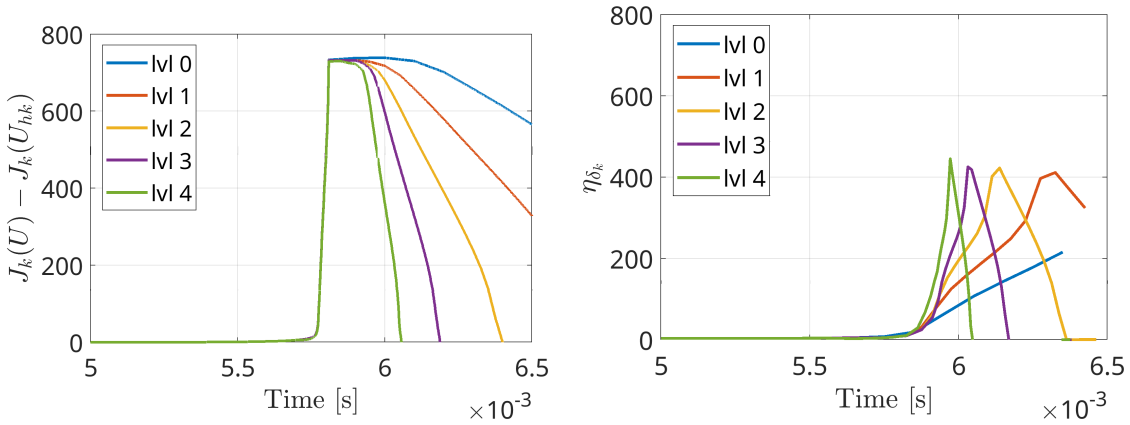

Figure 6: Zoomed in view of the exact error (left) and the estimated error (right) for adaptive refined temporal meshes.

The low estimate of the error at crack initiation is also affecting the quality of the estimator, as observed for the error indicators reported in Table 2. Contrary to the estimator with global refinements, the indicators do not tend toward 1 and remain at levels of about 0.2.

Table 2: Comparison of the estimated error, the exact error and the error indicators for different globally refined temporal meshes. The goal value of the reference discretization is 2.261.

Ref. level	0	1	2	3	4
$J(U_{hk})$	2.753	2.683	2.565	2.473	2.412
$J(U_h) - J(U_{hk})$	0.492	0.422	0.304	0.213	0.151
η	0.047	0.081	0.064	0.040	0.027
I_{eff}	0.094	0.192	0.211	0.190	0.182

7 Conclusion and outlook

In this work, goal-oriented temporal error control and adaptivity were introduced employing the dual-weighted residual method for phase-field fracture. First, a space-time framework was formulated as well as the corresponding space-time Galerkin finite element discretization. Having a goal functional at hand, an error estimator was derived for the temporal discretization error measured in the goal functional. These developments were substantiated with the help of a numerical test, namely, a single edge notched tensile test. Therein, the crack initiates first (very) slowly and then propagates in a (very) fast manner. Thus, this configuration is a good setting for temporal adaptivity. The performance was evaluated in terms of the final goal functional values, the reduction of the (true) error with respect to a numerically computed reference solution, the reduction of the error estimator, and, last effectivity indices that measure the fraction of true error and the estimator error. The current findings are promising by showing good effectivity indices on temporally adapted meshes. In ongoing work, the error estimator is extended to full space-time adaptivity (i.e., in time and space).

8 Acknowledgment

The financial support of the French-German University through the French-German Doctoral college "Sophisticated Numerical and Testing Approaches" (CDFA-DFDK 19-04) is acknowledged. Discussions are also acknowledged within the framework of the International Research Training Group on Computational Mechanics Techniques in High Dimensions GRK 2657 funded by the German Research Foundation (DFG) under Grant Number 433082294.

References

[1] Marreddy Ambati et al. "A review on phase-field models of brittle fracture and a new fast hybrid formulation". English. In: *Computational Mechanics* 55.2 (2015), pp. 383–405.

[2] Daniel Arndt et al. "The deal.II finite element library: Design, features, and insights". In: *Computers & Mathematics with Applications* 81 (2021), pp. 407–422.

[3] Daniel Arndt et al. "The `deal.II` Library, Version 9.4". In: *Journal of Numerical Mathematics* 30.3 (2022), pp. 231–246.

[4] Roland Becker and Rolf Rannacher. "An optimal control approach to a posteriori error estimation in finite element methods". In: *Acta Numerica* 10 (2001), pp. 1–102.

[5] Michael Besier and Rolf Rannacher. "Goal-oriented space-time adaptivity in the finite element Galerkin method for the computation of nonstationary incompressible flow". In: *Int. J. Num. Meth. Fluids* 70 (2012), pp. 1139–1166.

[6] Blaise Bourdin and Gilles A. Francfort. "Past and present of variational fracture". In: *SIAM News* 52.9 (2019).

[7] Blaise Bourdin et al. "The Variational approach to fracture". In: *J. Elasticity* 91.1–3 (2008), pp. 1–148.

[8] Patrick Diehl et al. "A comparative review of peridynamics and phase-field models for engineering fracture mechanics". In: *Computational Mechanics* 69 (2022), pp. 1259–1293.

[9] Lukas Failer and Thomas Wick. "Adaptive time-step control for nonlinear fluid-structure interaction". In: *Journal of Computational Physics* 366 (2018), pp. 448–477.

[10] Timo Heister and Thomas Wick. "pfm-cracks: A parallel-adaptive framework for phase-field fracture propagation". In: *Software Impacts* 6 (2020), p. 100045.

[11] Timo Heister et al. "A primal-dual active set method and predictor-corrector mesh adaptivity for computing fracture propagation using a phase-field approach". In: *Computer Methods in Applied Mechanics and Engineering* 290 (2015), pp. 466–495.

[12] Uwe Köcher et al. "Efficient and scalable data structures and algorithms for goal-oriented adaptivity of space–time FEM codes". In: *SoftwareX* 10 (2019), p. 100239.

[13] Charlotte Kuhn and Ralf Müller. "A continuum phase field model for fracture". In: *Engineering Fracture Mechanics* 77.18 (2010). Computational Mechanics in Fracture and Damage: A Special Issue in Honor of Prof. Gross, pp. 3625–3634.

[14] Nicolás A. Labanda et al. "A spatio-temporal adaptive phase-field fracture method". In: *Computer Methods in Applied Mechanics and Engineering* 392 (2022), p. 114675.

[15] Dominik Meidner and Thomas Richter. “A posteriori error estimation for the fractional step theta discretization of the incompressible Navier-Stokes equations”. In: *Comput. Methods Appl. Mech. Engrg.* 288 (2015), pp. 45–59.

[16] Dominik Meidner and Thomas Richter. “Goal-oriented error estimation for the fractional step theta scheme”. In: *Comput. Methods Appl. Math.* 14.2 (2014), pp. 203–230.

[17] Chrisitan Miehe et al. “Thermodynamically consistent phase-field models of fracture: variational principles and multi-field FE implementations”. In: *Int. J. Numer. Methods Engrg.* 83 (2010), pp. 1273–1311.

[18] Karsten Paul et al. “An adaptive space-time phase field formulation for dynamic fracture of brittle shells based on LR NURBS”. In: *Computational Mechanics* 65 (Apr. 2020).

[19] Rolf Rannacher and Franz-Theo Suttmeier. “A posteriori error estimation and mesh adaptation for finite element models in elasto-plasticity”. In: *Computer Methods in Applied Mechanics and Engineering* 176.1-4 (1999), pp. 333–361.

[20] Thomas Richter and Thomas Wick. “Variational localizations of the dual weighted residual estimator”. In: *Journal of Computational and Applied Mathematics* 279 (2015), pp. 192–208.

[21] Felix Rörentrop et al. *A time-adaptive finite element phase-field model suitable for rate-independent fracture mechanics*. 2024.

[22] Julian Roth et al. In: *Comput. Methods Appl. Math.* 24.1 (2024), pp. 185–214.

[23] Michael Schmich and Boris Vexler. “Adaptivity with Dynamic Meshes for Space-Time Finite Element Discretizations of Parabolic Equations”. In: *SIAM Journal on Scientific Computing* 30.1 (2008), pp. 369–393.

[24] Franz-Theo Suttmeier. *Numerical solution of Variational Inequalities by Adaptive Finite Elements*. Vieweg+Teubner, 2008.

[25] Jan P. Thiele and Thomas Wick. “Numerical Modeling and Open-Source Implementation of Variational Partition-of-Unity Localizations of Space-Time Dual-Weighted Residual Estimators for Parabolic Problems”. In: *Journal of Scientific Computing* 99.1 (2024).

[26] Thomas Wick. In: *Computational Methods in Applied Mathematics* 21.3 (2021), pp. 693–707.

[27] Thomas Wick. “Goal functional evaluations for phase-field fracture using PU-based DWR mesh adaptivity”. In: *Computational Mechanics* 57.6 (2016), pp. 1017–1035.

[28] Thomas Wick. *Multiphysics Phase-Field Fracture: Modeling, Adaptive Discretizations, and Solvers*. Berlin, Boston: De Gruyter, 2020.

[29] Jian-Ying Wu et al. “Phase field modelling of fracture”. In: *Advances in Applied Mechanics* 53 (Sept. 2019), pp. 1–183.

[30] Vahid Ziaei-Rad and Yongxing Shen. “Massive parallelization of the phase field formulation for crack propagation with time adaptivity”. In: *Computer Methods in Applied Mechanics and Engineering* 312 (2016). Phase Field Approaches to Fracture, pp. 224–253.